https://doi.org/10.2352/ISSN.2470-1173.2019.16.3DMP-003

3D Microscopic Imaging using Structure-from-Motion

Lukas Traxler, Svorad Štolc; AIT Austrian Institute of Technology; Vienna, Austria

Abstract

This work experimentally demonstrates inline 3D imaging using Structure-from-Motion in microscopic domain. Several microscopic 3D inspection systems exist. A popular method for standard microscopes is Depth-from-Focus reconstruction, which makes use of the shallow depth of field of microscope optics. It requires several scans acquired at different distances of the object along the optical axis. This and other 3D reconstruction methods based on a scanning process are not suitable for fast inline inspection if the scanning direction does not match the object's transport direction. In this paper we propose a modification to standard microscope optics, which allows for Structure-from-Motion in microscopic domain, by including an additional aperture. The choice of aperture opening and location is crucial to reach the desired lateral and depth resolution. This paper investigates the optimal choice for these parameters to match a desired application, in this case the inspection of a metallic surface with 4 µm resolution in all three dimensions. The choice based on theoretical considerations is successfully tested in an experimental setup. Results are compared with a reference measurement from confocal microscopy.

Introduction

Various manufacturing and quality control processes require inline 3D acquisition and measurements. Precision manufacturing or microelectronic applications demand resolutions in the μm–range. Several methods for microscopic 3D reconstruction exist: *Depth-from-Focus (DfF)* makes use of the shallow depth of field of typical microscope optics. 3D information can be extracted by acquiring an image stack at different distances along the optical axis [2][3]. As the scanning direction along the optical axis does not match the transport direction of the object to be inspected, this technique is not well suitable for inline inspection applications. Other than that different optical setups can be used: *White Light Interferometry (WLI)* makes use of low coherence of broadband white light sources. Interference only occurs if path length delay between the object ray and a reference ray is within the short coherence time. The coherence time determines the depth resolution, independent from the field of view. This makes WLI suitable for precise depth measurements for large fields of view. Still, as for SfF, the depth information can only be acquired by a scanning process, e.g. scanning for different reference path lengths [1]. Typical industrial inline WLI implementations require cycle times around several hundred ms per square mm. In *Confocal Microscopy (CM)* typically each 3D point in x,y,z space is scanned separately [1], again preventing the comfortable implementation in inline applications. With line scan chromatic CM it is possible to encode the depth information into wavelength allowing for a non-stop inline 3D acquisition [4], but with the cost of a higher system complexity. *Structure-from-Motion (SfM)* acquisition techniques are well tested for macroscopic objects [5], but until now not investigated in the microscopic domain.

Prior Work

In prior work we demonstrated that multi–line scan cameras are highly suited for fast inline acquisitions [6]. When an object passes by the camera each sensor line corresponds to a view of the object form a different observation angle. This method is beneficial as only a single camera and a conventional endocentric imaging lens is needed. The method can be seen as a special case of a SfM 3D acquisition process with precisely known camera poses and equivalent set of viewing angles for each observed object point. The 3D information is deduced from a linear light-field image stack, thus a texture map can be generated from the same acquisition process. Recent work in line-scan camera calibration makes this approach also suitable for measurement tasks [7].

The depth resolution of these systems is determined by the stereo baseline, the angle between the utmost views. The lateral resolution is determined by the imaging optics, camera and transport speed. Adapting our prior work to microscopic scale of μm–resolution entails some challenges: (i) high lateral resolution used in microscopy implies low depth of field; (ii) typical microscopic optics are designed to have telecentric perspective, which means that no parallax or change in viewing angle is generated from different field points, thus 3D information can't be gathered from motion. This paper proposes a simple modification to an industrial inspection microscope optic to make it suitable for microscopic SfM 3D reconstruction, which enables precise 3D measurements in a non-stop inline acquisition in addition to a texture map.

Optical Configuration

As addressed above, standard microscope optics are not suited for SfM for two reasons: (i) the shallow depth of field prevents to capture the full 3D structure (ii), the telecentric optics maintain the same perspective regardless of the field position. We propose a modification of the microscope optics that solve both these issues at once: The depth of field is extended by introducing an additional aperture with a reduced diameter. As depicted in Figure 1 the position of the aperture determines the perspective property of the optical system. Placing the aperture in the back focal plane of the objective lens (see Figure 1, AP_{tele}), this is the typical construction of a microscope objective, forces the central ray of any light cone, regardless of the field position, to go through the focal point of the objective lens and thus resulting in a central ray parallel to the optical axis in object space. If stopping down the aperture at the telecentric position (see Figure 1, AP_{tele}), only the central zone of the objective lens would be used and only a small part of the wide aperture objective is used,

but depth of field (DOF) increases. By changing the perspective properties, one can now make use of the outer rim for oblique perspective views on the object. This is done by moving the additional aperture to another location (see Figure 1, AP_{hyper}). Using a hypercentric projection, off axis field points are viewed through the outer zone of the objective lens. Increasing the distance between the objective lens and the aperture plane AP_{hyper} increases the hypercentric perspective, resulting in a better 3D stereo baseline compared to an aperture position closer to the telecentric position. This is possible as long as the objects light cone is not vignetted by objective lens original aperture (NA_{full}).

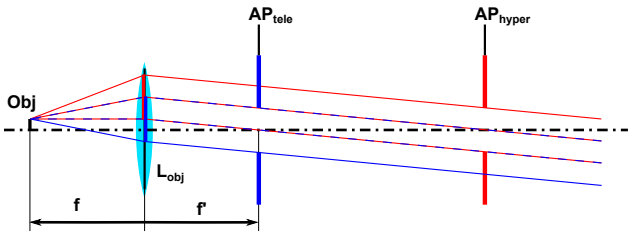

Figure 1. *A microscope objective lens (L_{obj}) is stopped down by an additional aperture (AP) to increase the DOF. If the aperture is positioned behind the objective's focal plane the (AP_{hyper}), a hypercentric perspective is generated. While in telecentric perspective (blue) the object is always observed from the same direction, in hypercentric perspective (red) the object can be observed from a slanted light cone at the outer fraction of the lens; here the central ray is not parallel to the optical axis.*

Hypercentric perspective is opposite to the conventional endocentric projection. For a hypercentric system the projection center lies behind the object, thus objects which are further away from the imaging system appear in a higher magnification and thus move faster if the object is transported perpendicular to the optical axis. This effect is illustrated in Figure 2.

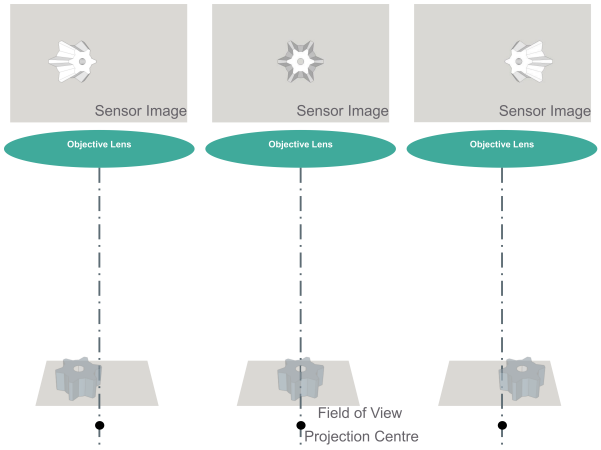

Figure 2. *Visualization of a hypercentric projection: An object is transported from left to right through the field of view. The upper row depicts the images captured by the microscope camera for the case of hypercentric projection. As the projection center lies behind the object, the back plane of the object appears bigger and moves faster in the image than the front plane.*

Hypercentric projection is beneficial compared with endocentric perspective: For an endocentic projection with the same stereo baseline as demonstrated in this paper, the aperture would have to be placed close (about 5 mm) to object . This causes practical problems due to a reduced working distance of the optical system for inline applications, and the aperture mounting would interfere with the illumination light path.

Analysis of the Aperture Position and Location

To find optimal values for the aperture position d (distance between objective lens and additional aperture) and the aperture diameter D, a simplified model of the microscope system with the additional aperture (see Figure 3) is modeled in ZEMAX OpticStudio. From that, all imaging parameters are deduced. The aperture diameter D influences the optical resolution. For microscopic application, commonly the aperture opening is expressed by the *numerical aperture NA*. Introducing an additional aperture in the ray–path between objective and tube lens, results in a NA of:

$$NA = \sin\left(\arctan\left(\frac{D}{2f'}\right)\right) \tag{1}$$

Where f' is the objective's focal length, for an infinite corrected microscope the objective's focal length depends on the tube focal length f'_{tube} and magnification M:

$$f' = \frac{f'_{tube}}{M} \tag{2}$$

For well corrected high-quality microscope objectives the lateral resolution is determined by the diffraction limit. Using the Rayleigh resolution criterion the lateral resolution can be expressed by:

$$Res_{xy} = \frac{0.61\lambda}{NA} \tag{3}$$

As the microscope is applied for imaging 3D structures it has to be emphasized that the structures stay within the depth of field. The depth range, for which stereo matching is still possible, is deduced from the optical model and can also be expressed by the system's NA:

$$DOF = \pm\frac{\lambda}{NA^2} \tag{4}$$

The depth resolution Res_z is calculated by assuming that the smallest height difference can be detected if the resulting parallax between the two outermost oblique views along the transport direction $\pm\alpha_t$ is at least one pixel. For a sensor resolution of n_t pixels in transport direction geometrical analysis leads to a stereo depth resolution Res_z of:

$$Res_z(\alpha_t) \approx \frac{f'}{n_t\left(\frac{d}{f'}-1\right)} = \frac{f'^2}{n_t(d-f')} \tag{5}$$

Finally the condition preventing vignetting can be formulated in an inequality:

$$\frac{y_d}{M} < \frac{f'^2}{d}(NA_{full} - NA) \tag{6}$$

Fulfilling this inequality, the captured light cone of an object points at the corners of the field of view (diagonal field height of y_d) still goes entirely through the full, unmodified aperture of the objective lens (NA_{full}).

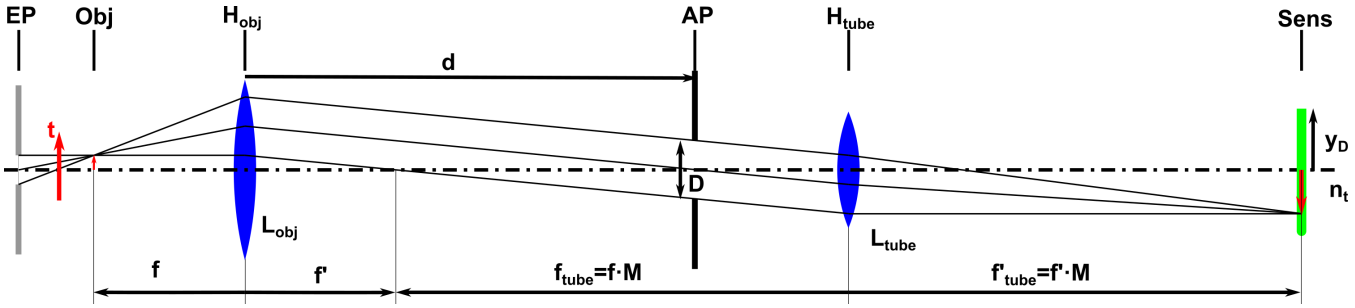

Figure 3. *Simplified model of the microscope optics containing an objective lens (L_{obj}) and tube lens (L_{tube}). An aperture (AP) is placed in the distance (d) to the objective lens. Its virtual image is the entrance pupil (EP). The object position (Obj) is a conjugate plane to the sensor (Sens). For inline inspection the object travels along the transport direction (t). The image sensor has n_t pixels in transport direction and a sensor diagonal of y_D.*

Choice of Aperture Position and Location

To demonstrate the practical applicability, choosing useful values for d and D is shown for the application example of 3D metallic surface inspection. In the demonstrated application shallow ($<$70 μm) embossings on a 20 Euro cent coin are investigated.

An industrial machine vision microscope (”Infinity InfiniTube” tube system with a Mitutoyo 10$\times$ objective with $NA = 0.28$, $f' = 20$ mm and a long working distance of $WD =$ 33.5 mm) is used for the experiments presented in this paper. The objective lens has a specified resolving power of 1 μm). A high–speed color camera (Bonito CL-400C) with 7 μm pixels and 16.24 mm $\times$ 12.08 mm sensor size is used for image acquisition. According to the formulas provided above the optimal configuration for a specific application can be found as follows:

For the chosen camera the diagonal filed height calculates to: $y_d = \sqrt{(16.24\text{mm}/2)^2 + (12.08\text{mm}/2)^2} = 10.12$ mm. Choosing an aperture distance of $d = 78$ mm, Eq. (6) allows for maximal NA of 0.083. Stopping down to $NA = 0.083$ increases the DOF to $\pm$80 μm Eq. (4) and results in a lateral optical resolution of 4 μm Eq. (3). The 10$\times$ magnification results in a lateral sampling of 700 nm. The depth resolution for the maximal perspective parallax in transport direction is 4 μm.

By choosing a larger d, causing a better Res_z Eq. (5), results in a smaller NA Eq. (6) and thus in a worse Res_{xy} Eq.(3). In general this implies that depth resolution Res_z and lateral resolution Res_{xy} counteract each other, a compromise where $Res_z = Res_{xy}$ was chosen. If the results do not fulfill the required acquisition properties, either the choice of camera or choice of imaging lens can help to increase the system performance: To further increase the depth resolution, a camera with a larger resolution especially higher number of pixels in transport direction n_t Eq. (5) has to be chosen. For practical reasons one is limited to a particular pixel size for obtaining sufficient light in a fast inline acquisition process. Alternatively, the amount hypercentric perspective, thus the stereo baseline, can be increased by increasing d. The participial limit in this case is, that d can only be increased until vignetting occurs Eq. (6). Therefore it is beneficial if the unmodified objective lens supports a high numerical aperture NA_{full}.

The optical modifications induce lens distortions; thus an image rectification is done using OpenCV with an algorithm based on [8, 9]. For an inline light field acquisition a suitable camera calibration and image rectification is shown in [7]. For subsequent 3D reconstruction a standard SfM algorithm was used. As the aperture location also influences the lens distortions, the proposed modification induces additional lens distortions. Prior to applying the SfM algorithm images are corrected for schading (i.e. so called flat field correction) and undistorted.

Pinhole Camera Model

The camera calibration routine and SfM algorithm assume a pinhole camera model. The pinhole camera model used in this paper is depicted in Figure 4 (upper model). The entrance pupil (EP) is the image of the aperture (AP) through the objective lens, which defines its location. As it can be seen in Figure 3, the EP is behind the object. This is expressed by a negative sign of p. Given a defined magnification M, the focal length of the pinhole camera can be defined by: $f_p = -p \cdot M$. Standard camera calibration

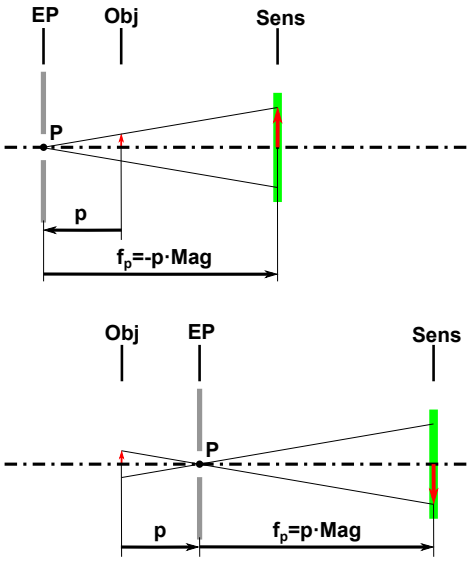

Figure 4. *Upper model: Pinhole camera model for the proposed hypercentric microscope setup: The location of the entrance pupil (EP) defines the camera's pinhole (P) which is behind the object. The pinhole camera's focal length f_p results from the magnification M. Lower model: analogous classical endocentric pinhole camera model with the projection center between the object and the camera sensor.*

and SfM algorithms assume an endocentric perspective projection as depicted in 4 (lower model). In that case p is positive. The SfM algorithm can not distinguish between a hypercentric or endocentric perspective. Using the algorithms' assumption of an endocentric projection (positive p) the z-coordinate (depth) has to be flipped to account for the negative p inherent in the proposed acquisition setup. Beside that, no special treatment is needed for the hypercentric system.

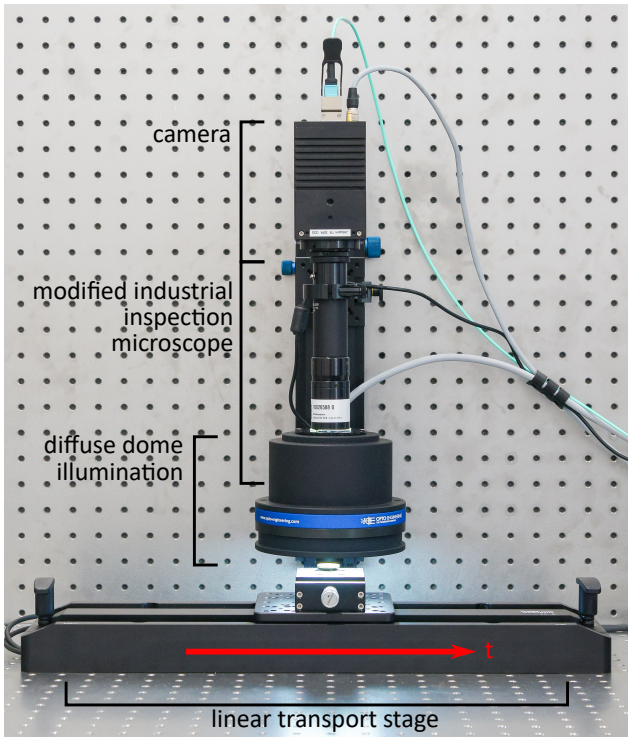

Figure 5. *Experimental setup for the microscopic 3D inspection system. The red arrow (t) indicates the transport direction.*

Experimental Results

Figure 5 depicts our experimental setup. A diffuse ring light and indirect dome illumination is used. The diffuse illumination is chosen to ensure a consistent reflectance regardless of the viewing angle, this improves the correspondence analysis performed by the SfM algorithm.

Camera Calibration

For calibration a dot-grid target with 125 μm grid spacing is presented in 15 different orientations in front of the camera, so that the full field of view and DOF of the acquisition volume is covered by calibration points. In total across all images 1870 points are used for calibration. For the camera model depicted in Figure 4 the intrinsic calibration results in a focal length of $f_p = 5491.7$ pixels $= 38.44$ mm. From the extrinsic camera calibration the poses of the presented calibration charts are known (see Figure 6). Selecting the in-focus calibration dots, p can be estimated from the extrinsic calibration, where $p = 4.20$ mm (note: the p is positive as the camera model assumes an endocentric projection). This suggests a magnification of $M = f_p/p = 9.15$. The slight deviation from the theoretical 10$\times$ magnification can be explained as in the InfiniTube system the tube lens is split into two lens groups, where the second group is movable to adjust the focus, this adjustment changes the effective focal length of the tube lens.

3D Metrology

To demonstrate a possible application in metal surface inspection with this experimental setup, a 20 Euro cent coin with a known reference measurement, obtained with CM, is acquired. This is done for two 1.4 $\times$ 1.4 mm ROIs within the coin (see Figure 7). For each ROI 25 images are acquired with a transport increment of 100 μm. This sequence 25 subsequent images is fed into the SfM algorithm, the central 1.4 $\times$ 1.4 mm region is cropped from the 3D reconstructions. Results are depicted in Figure 8 (ROI 1) and 9 (ROI 2). 3D reconstruction obtained by our system are registered to a CM measurement for validation. The deviation between measurement and reference shows a mode of 5 μm in ROI 1 a mode of 2 μm in ROI 2. The difference between the error distributions in both ROIs is discussed below. For ROI 2 the standard deviation of the error is 3.2 μm and thus below the optical resolution of the system.

Discussion and Outlook

In both ROIs the mode of the absolute deviation (5 μm / ROI 1 and 2 μm / ROI 2) is in the same magnitude as the optical resolution of the system ($Res_z \approx Res_{xy} = 4\mu$m). In ROI 1 there is a larger deviation in the lower leg of the letter 'E', which

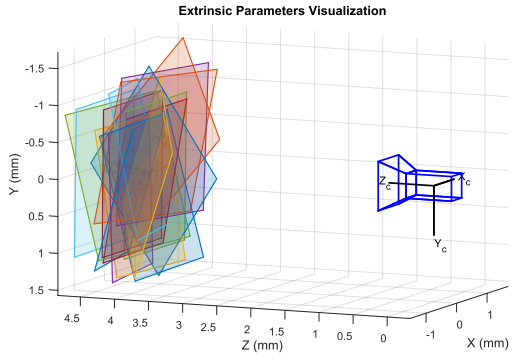

Figure 6. *Visualization of the 15 poses used to calibrate the imaging system. Selecting the in-focus calibration points, the location of the projection center $p = 4.20$ mm can be deduced experimentally.*

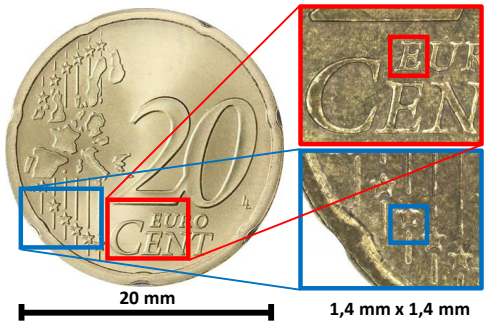

Figure 7. *Position of the two 1.4 $\times$ 1.4 mm ROIs (small squares) for demonstrating metal surface inspection: ROI 1 – letter 'E' with aproximately 1 mm letter height; ROI 2 – star embossing*

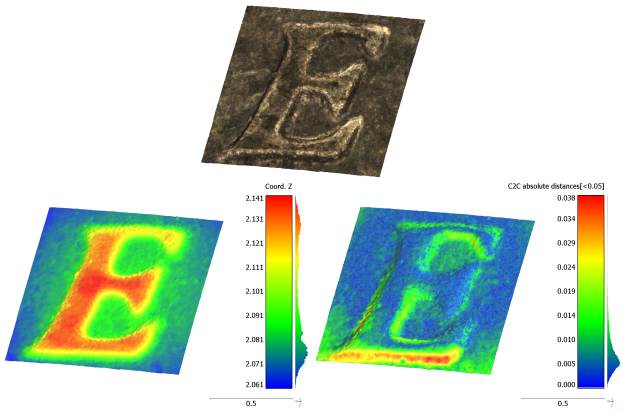

Figure 8. *Results ROI 1: top – texture image; bottom left – depth map; bottom right – difference to reference measurement. Unit: mm*

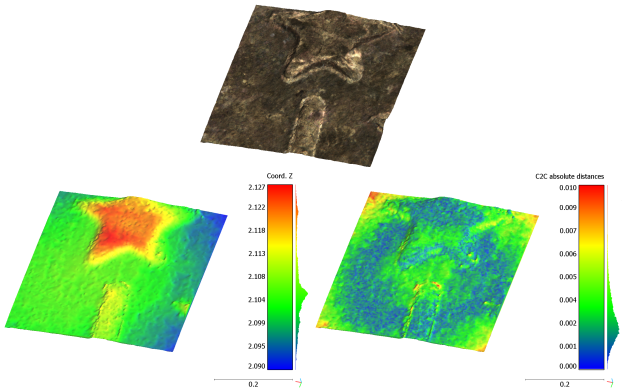

Figure 9. *Results ROI 2: top – texture image; bottom left – depth map; bottom right – difference to reference measurement. Unit: mm*

results from an artifact in the provided reference measurement. As depicted in Figure 10 there is an obvious scanning offset artifact in the data from CM.

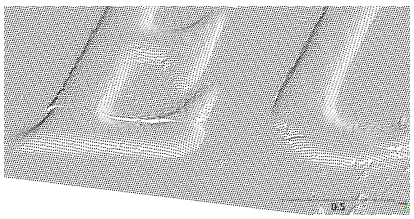

Figure 10. *Point cloud of the confocal microscopy reference measurement, a scanning artifact is visible in the lower leg of the letter 'E'.*

In the sample with the shallow embossing (see Figure 9), a ring-like deviation pattern is visible. The artifact has a peak deviation of 8 μm (twice the optical resolution) at the edge of the FOV. This phenomenon is systematically visible in all acquisitions and results from a slightly inaccurate lens distortion model, which lets flat surfaces appear bent. With a more elaborate camera calibration, e.g. accounting for chromatic aberration, and incorporating the pre-knowledge on the camera poses, currently not taken into account by the SfM algorithm, this systematic error can be eliminated. Even without this correction it can be demonstrated that the standard deviation of the error is smaller than the optical resolution of the system.

This work experimentally demonstrates that an inline 3D imaging using SfM is also feasible for microscopic applications. This method is of interest as 3D maps and texture maps can be acquired at the same time in a non-stop inline acquisition process. Compared to other methods such as SfF, WLI or CM, in the presented approach the objects only pass by the objective lens laterally. Providing sufficient light synchronously strobed to the object's transport, 3D structures can be acquired in single continuous transport. With available light sources rapid 3D inspections are possible with scanning speeds up to 10 mm/s for the demonstrated field of view and resolution.

References

[1] M. Novak, D. Sharma; 3-D Optical Microscopes: A Basic Technology Comparison for Metrology Applications; Quality - Test & Inspection; 2013

[2] M. Muhammad and T. Choi; Sampling for Shape from Focus in Optical Microscopy; IEEE Transactions on Pattern Analysis and Machine Intelligence, vol. 34, no. 3, pp. 564-573; March 2012

[3] I. T. Young, R. Zagers, L. J. van Vliet, J. Mullikin, F. Boddeke, H. Netten; Depth-of-focus in microscopy; Proceedings of the Scandinavian Conference on Image Analysis. Vol. 1; 1993

[4] J. Sepp, K. Niemel, A. Lassila; Metrological characterization methods for confocal chromatic line sensors and optical topography sensors; Meas. Sci. Technol. 29 054008, 2018

[5] State-of-The-Art and Applications of 3D Imaging Sensors in Industry, Cultural Heritage, Medicine, and Criminal Investigation, Sensors (Basel), 9(1), 2009

[6] S. Stolc et al., Depth and all-in-focus imaging by a multi-line-scan light field camera, Journal of Electronic Imaging, 23(5), 2014.

[7] B. Blaschitz, S. tolc, D. Antensteiner; Geometric calibration and image rectification of a multi-line scan camera for accurate 3D reconstruction; IRIACV, 240-1-240-6(6); 2018

[8] Z. Zhang; A flexible new technique for camera calibration; IEEE Transactions on Pattern Analysis and Machine Intelligence, 22(11):1330-1334; 2000

[9] J. Bouguet; Camera Calibration Toolbox for MATLAB; `http://www.vision.caltech.edu/bouguetj/calib_doc/`; 2004

Author Biography

DI Dr. Lukas Traxler, earned his PhD in Technical Physics in 2018 and his master's degree in Biomedical Engineering in 2014 both at the Technical University of Vienna, Austria. He joined the AIT Austrian Institute of Technology at the Center for Vision, Automation & Control in 2017 where his main research focus lies on optics and computer vision. Since 2014 he teaches at the University of Applied Sciences Technikum Wien, Austria.

Dr. Svorad Štolc is a senior scientist in the Center for Vision, Automation & Control of the AIT Austrian Institute of Technology GmbH, Vienna. He graduated in Computer Science from Comenius University, Bratislava and earned his PhD degree in Bionics and Biomechanics from Technical University of Košice. Since 2018 at AIT, he coordinates research activities in high–speed sensing, inline computational imaging and machine learning with the focus on industrial inspection and document security. He is a (co)author of more than 50 peer-reviewed scientific papers and holds a number of patents in machine vision.

JOIN US AT THE NEXT EI!

IS&T International Symposium on

Electronic Imaging

SCIENCE AND TECHNOLOGY

Imaging across applications . . . Where industry and academia meet!

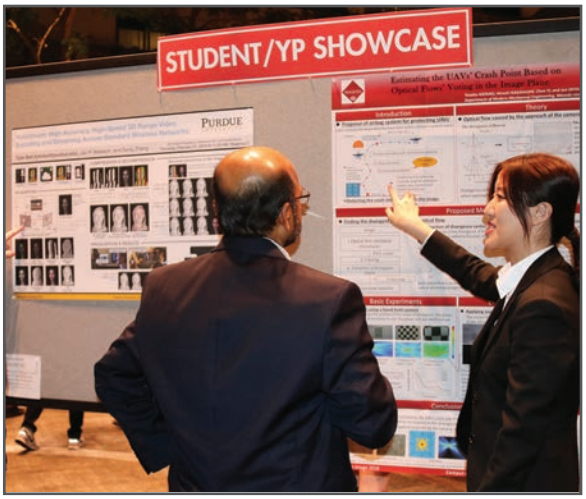

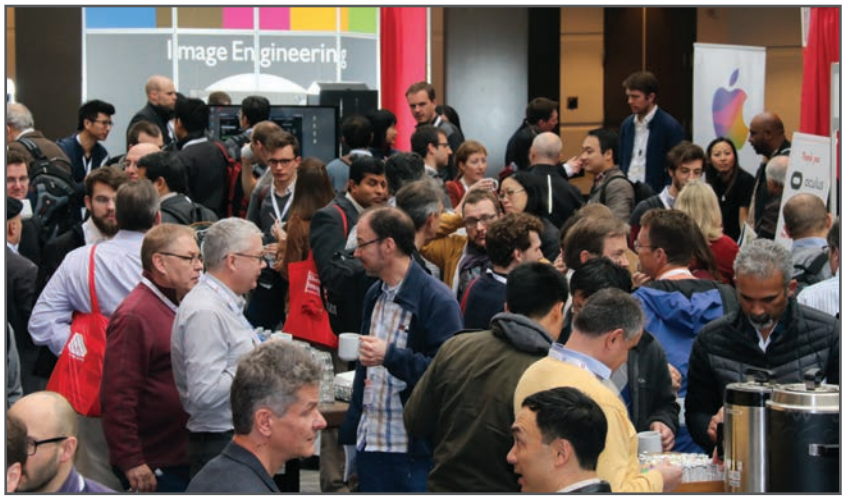

• SHORT COURSES • EXHIBITS • DEMONSTRATION SESSION • PLENARY TALKS •
• INTERACTIVE PAPER SESSION • SPECIAL EVENTS • TECHNICAL SESSIONS •

www.electronicimaging.org

IS&T
imaging.org